5
Formation of heterojunction via surface decoration for enhanced formaldehyde detection

This chapter describes the detailed about fabrication process of n-n ZnO/SnO_2 and p-n NiO/SnO_2 heterojunction based metal oxide sensor to explore the formaldehyde sensing behaviour. In the previous chapter 4, we already discussed about the synthesis process of n-type ZnO nanoparticles using pulse laser ablation method. In this chapter, we described the fabrication of n-n ZnO/SnO_2 heterojunction by the surface decoration of sputtered deposited SnO_2 thin film with laser ablated ZnO nanoparticles (NPs). In the beginning, we will show the surface decoration method on SnO_2 thin film using ZnO colloidal solution via drop casting method directly using a micropipette. Moreover, we will explore the various gas sensing properties such as sensitivity, selectivity, short- and long-term reliability of the fabricated n-ZnO/n-SnO_2 heterojunction sensor towards formaldehyde gases. Furthermore, our focus is to develop a p-n heterojunction based metal oxide sensor and explore the formaldehyde sensing capabilities with high sensitivity and selectivity. It is already reported that p-type NiO is a very good functional material to improve the sensitivity and selectivity of the formaldehyde gas. So, in this chapter, we described the synthesis process of p-type NiO metal oxide nanoparticles by surface ablation of pure (99.99%) Ni pellet in ambient air using UV laser (355 nm wavelength) beam and obtained NiO nanoparticles were used to decorate the surface of SnO_2 thin film to fabricate p-n NiO/SnO_2 sensor. Further, the fabricated NiO/SnO_2 sensor was exposed to formaldehyde gas and various gas sensing parameters such as operating temperature, static response, limit of detection (LoD), short- and long-term reliability, etc. were extracted from the test results.

5.1 Introduction

Till to date, nanostructured SnO_2 thin film based metal oxide gas sensors are used for the detection of low concentration levels of formaldehyde gas with higher sensitivity and good stability over a long period of time due to some inherent properties such as low cost, excellent sensitivity, quick response and recovery time [Dey, 2018][Chen et al., 2015][Chung et al., 2013][Allouch et al., 2013][Das et al., 2014][Li et al., 2019b] [10–12]. But, SnO_2 based metal oxide sensors are suffering from the selectivity issues towards formaldehyde gases and it is still a challenging issue for researchers [Simon et al., 2001]. To overcome this challenge, researchers are trying to implement various strategies. Among them, making heterojunction based (n-n or p-n) metal oxide sensors using the surface decoration technique is one of the most proven techniques as reported by many research articles. For the surface decoration of thin or thick film metal oxide, nanostructured metal oxide materials with various shapes and surface morphologies such as nanorods, nanowires, nanobelts, nanospheres, nanoparticles (NPs) have been used [Castro-Hurtado et al., 2013][Joshi et al., 2018][Giberti et al., 2016] [Yu et al., 2019b]. At recent, huge efforts have been given for the development of heterojunction based formaldehyde sensors by modifying the surface of the n-type SnO_2 layer with n-type (ZnO) and p-type (CuO, NiO, AgO, etc.) metal oxide to form n-n and p-n heterojunction [Du et al., 2012][Xiao et al., 2015][Meng et al., 2018b]. For example, Lou C et al. [Lou et al., 2021] developed n-n heterojunction-based formaldehyde sensor by modifying n-type SnO_2 heterospheres with n-type ZnO materials using the atomic layer deposition (ALD) technique. The developed metal oxide sensor showed a gas response of 38.2 towards 20 ppm formaldehyde gas with fast response (17 s) and recovery time (25 s) with excellent stability over 28 days. For example, Zhu Li Yuan et al. [Zhu et al., 2019b] developed p-CuO/n-SnO_2 heterojunction-based formaldehyde sensors and obtained a good response of about 2.42 towards 50 ppm formaldehyde gas at temperature of 250°C. K. Khamfoo et al. [Khamfoo et al., 2020] fabricated a formaldehyde

sensor by doping n-type SnO_2 nanoparticles with p-type AgO using flame spray pyrolysis process and they
obtained a response of 495 to 2000 ppm formaldehyde at 350°C. G. Zhang et al. [Zhang et al., 2016] also fabricated NiO/SnO_2 p-n heterojunction based sensor by an electrospinning process and obtained an excellent response of 20 towards 100 ppm formaldehyde at an operating temperature of 200°C with good selectivity.

But, most surface modification techniques of metal oxides follow chemical synthesis routes, in which toxic chemical precursors are used to prepare the heterostructures [Xing et al., 2017]. It has been found that these processes are time-consuming and leave some chemical residue in the synthesized nanoparticles (NPs). So, a new rapid method is required for surface-decoration and doping of metal oxide nanostructures to develop low-cost gas sensors. Nowadays, pulse laser ablation (PLA) techniques are used for the synthesis of metal oxide nanoparticles (NPs) as an alternative to the chemical routes [Hongseok Choi, 2007]. In recent years, the synthesis of metal oxide nanoparticles (NPs) in air or liquid by laser ablation methods has been attractive to researchers for its potential applications in the gas sensing field [Fernández-Arias et al., 2020][Boutinguiza et al., 2015]. In this method, the NPs are produced by laser ablation of a solid source using femto- or nanosecond-laser [Boutinguiza et al., 2018]. The obtained nanoparticles show accurate stoichiometry with good crystallinity to their source material. Hence, pulse laser ablation (PLA) of solid sources provides an effective way to synthesize NPs without the need for toxic chemicals, vacuum chambers, and additional sophisticated vacuum controlling equipment. In this context, various researchers have already developed laser-ablated nanoparticles-based gas sensors. In the previous chapter 4, we have already reported a formaldehyde sensor based on ZnO nanoparticles using laser ablation techniques [Nanoparticles-based, 2021]. The sensor exhibited a detection limit of 50 ppm formaldehyde with 25 s response and 12 s recovery time. In addition, laser-ablated NPs can be used for surface decoration of metal oxides, and the gas sensing performance can be improved by changing their morphology, structure, size, and porosity. In the present chapter, the gas sensing behaviour of n-n heterojunction based metal oxide sensor was discussed by modifying the surface of sputtered deposited n-type SnO_2 thin film with laser ablated n-type ZnO nanoparticles by combined processes of physical vapor deposition (PVD) by sputtering for SnO_2 thin film and laser ablation technique for ZnO NPs.

Last few years, researchers are giving more attention to develop p-n heterojunction based sensors by combining p-type NiO and n-type SnO_2 material to improve sensitivity and selectivity towards formaldehyde gases [Allouch et al., 2013][Barsan et al., 2001a][Das et al., 2014][Tonezzer et al., 2018]. At present, the surface decoration method to form heterojunction by modifying the top the surface of n-type SnO_2 thin film with p-type NiO nanoparticles is drawing more attention among researchers [Wang et al., 2017]. So far, as a functional material for the improvement of selectivity towards formaldehyde gas, NiO material has been used for a long time due to its catalytic behaviour (oxidation of formaldehyde) and NiO material also enhances its selectivity and sensitivity to formaldehyde gases at lower working temperatures [Dirksen et al., 2001][Castro-Hurtado et al., 2011][Ju et al., 2014][Lou et al., 2021][Das et al., 2022][Zhang et al., 2016][Meng et al., 2018c]. Last few years, n-type SnO_2 material is decorated with NiO nanoparticles having various shapes (rods, particles, cubes, sheets, and so on) and various synthesis mechanism has been used such as pulse laser deposition (PLD)[Brilis et al., 2005][Ristoscu et al., 2007][Ju et al., 2015], drop casting [Fang et al., 2017], hydrothermal [Gu et al., 2017][Din et al., 2020][Pascariu et al., 2016], electrospinning [Zheng et al., 2011][Hu et al., 2018][Tang et al., 2016] etc. to produce NiO nanoparticles. The above synthesis methods need toxic chemicals and long-time to fabricate the real-time sensors. However, little attention has been devoted for searching an alternative chemical free synthesis route to produce NiO nanoparticles for the fabrication of sensing layer and surface modification.

The last few years, synthesis of metal oxide nanoparticles (CuO, AgO, ZnO, SnO_2, NiO etc.) in air or liquid via laser ablation technique using pure solid metals or metal oxide pellet is drawing more attention among researchers [Nedialkov et al., 2004][Hongseok Choi, 2007][Haupt et al., 2007][Boutinguiza et al., 2018][Fernández-Arias et al., 2020][Das et al., 2020].

Formaldehyde sensing properties via the formation of NiO/SnO_2 heterojunction based sensors are reported by several research articles but as per our best knowledge, synthesis of NiO nanoparticles in ambient air via laser ablation method using a pure Ni pellet has not been reported so far. So, in this chapter, we explored the formaldehyde sensing behavior of p-NiO/n-SnO_2 heterojunction based sensor via surface decoration of synthesized NiO NPs over sputtered deposited SnO_2 thin film.

5.2 Experimental details

5.2.1 Fabrication of n-ZnO/n-SnO_2 (n-n) heterojunction based sensors

First, a 40 nm thin SnO_2 layer was directly deposited on the top surface of a hollow ceramic tube with 4 mm in length, 0.8 internal and 1.2 mm external in diameter using the sputtering method (Figure 5.1 (a)). For the sputtering of SnO_2 thin film, a 99.99% pure SnO_2 target was used in the sputtering system (TFSP-840, VST Israel). During SnO_2 deposition in the chamber, Ar gas pressure was 7 mTorr and 100 W dc power was applied to the target. The schematic diagram is shown in figure 5.1 (b). During deposition of SnO_2 thin film, we also prepared some samples by depositing SnO_2 on the oxidized silicon substrates to analyse particle morphology and crystalline phase.

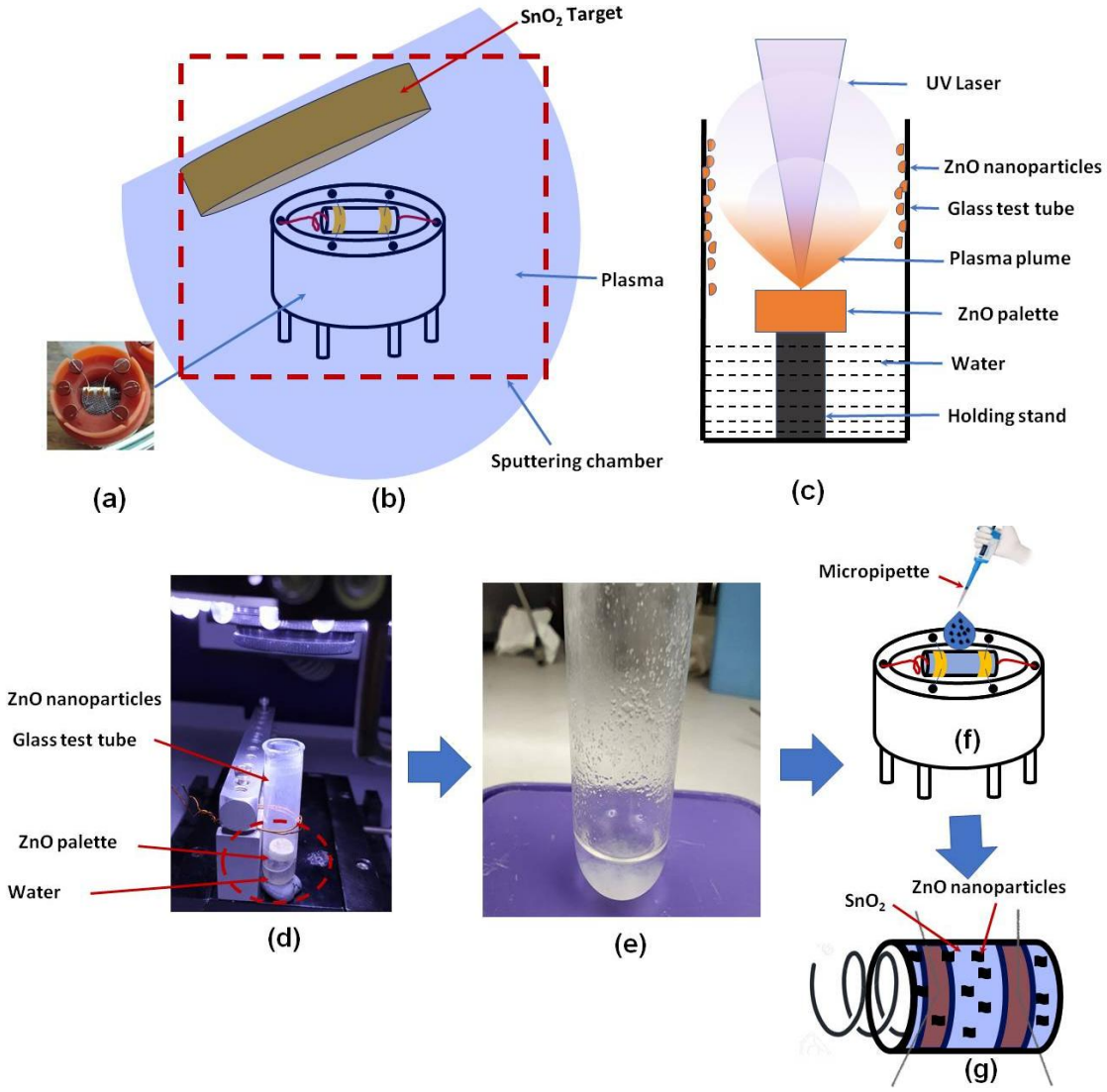

Figure 5.1: (a) Ni-Cr heater based gas sensor platform optical image. (b) Deposition of SnO_2 thin film on top of alumina tube gas sensor platform (Schematic). (c) Schematic of the laser ablation process. (d) ZnO pellet in test tube arrangement. (e) Laser ablated ZnO nanoparticles enriched colloidal solution (f) Decoration of ZnO NPs using drop casting method. (g) Decorated ZnO NPs on SnO_2 thin film (Schematic).

To decorate the SnO_2 thin film, ZnO nanoparticles based colloidal solution was produced. To synthesize the ZnO nanoparticles, a solid cylindrical shape polycrystalline ZnO pellet (99.9% pure) (American elements, USA) with 10 mm in diameter and 6 mm in height was used material. For the synthesis of ZnO pellet via laser ablation in open air ambient, a Q-switched Nd:YVO_4 laser (wavelength: 355 nm; pulse width: 20 ns; pulse repetition rate:30 KHz;) (Photonics Industries International Inc, USA) (Figure 5.1 (c)) was used. To collect the ZnO nanoparticles vapor, a test tube partially filled with 10 ml of DI water was used and the ZnO pellet was kept just above the water using a cylindrical rod stand in the glass test tube. The top surface of the ZnO pellet was aligned with the incident laser beam, as shown in figure 5.1 (d). During laser ablation, the laser beam power was focused on the upper surface of the ZnO pellet and the laser beam was scanned with 10 W power on a 3x3 mm^2 area using a high-speed galvo-scanner (speed of 60,000 mm/s). The detailed procedure of the laser ablation process of ZnO NPs has been discussed in our previous work [Nanoparticles-based, 2021]. When the laser beam irradiated on the ZnO surface, ZnO nanoparticles were ejected from the laser ablation process and ejected particles were deposited onto the inner wall of the glass test tube as a fine powder due to the condensation (Figure 5.1 (d)). Afterward, the glass test tube was shacken and the deposited fine powder of ZnO NPs in the glass test tube was dispersed in DI water and gradually, ZnO NPs enriched colloidal solution was prepared (Figure 5.1 (e)). Furthermore, form the high concentration of suspended ZnO NPs solution, we have prepared a dilute colloidal solution by adding some extra DI water. The as-deposited sputtered SnO_2 thin film on the ceramic tube substrate was decorated using laser ablated ZnO nanoparticles enriched colloidal solution via drop casting method directly using a micropipette (Borosil) as shown in figure 5.1 (f). After decoration the sample, it was kept a few hours at room temperature to dry the water vapor (Figure 5.1 (g)).

5.2.2 Fabrication of p-NiO/n-SnO_2 (p-n) heterojunction based sensors

A SnO_2 thin layer was deposited on an alumina tube based gas sensor platform as we fabricated in earlier chapter 4 of our thesis and the schematic diagram of the process is shown in figure 5.2 (a). The construction details of the gas sensor platform were already discussed in the previous chapter 3 [Das et al., 2022] and we have used the same gas sensor platform as we used in the previous case. The sputtering time, Ar gas pressure, applied RF power and other process parameters were the same as we reported earlier in chapter 4 [Das et al., 2022]. Here, our proposed plan is to synthesize NiO nanoparticles using laser ablation technique and synthesized NiO particles will be used for surface decoration of the SnO_2 layer.

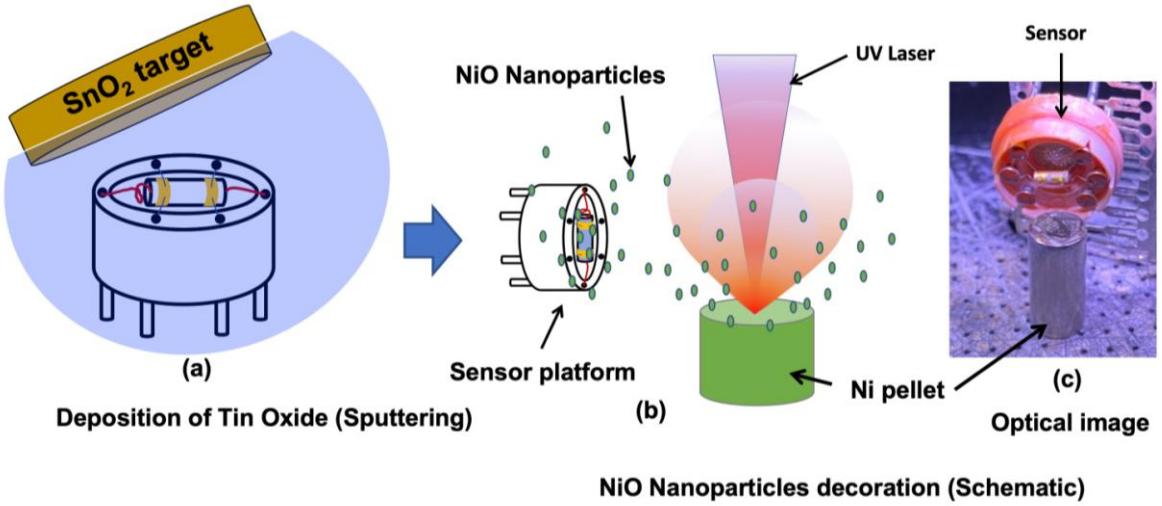

Figure 5.2: (a) Schematic of gas sensor platform in sputtering chamber. (b) Decoration of tin oxide thin film using laser ablated NiO Nanoparticles. (c) Optical images of gas sensor platform and cylindrical shape Ni pellet.

For the synthesis of NiO nanoparticles, a cylindrical shape 99.99% pure Ni pellet was used as a source of NiO material. Before the ablation process, the Ni metal pellet was cleaned with the standard RCA-1 cleaning method. In atmospheric air, laser beam of 355 nm wavelength was

bombarded on the top surface of Ni pellet with ~10 W power to synthesize NiO nanoparticles using a Q-switched Nd:YVO_4 based nanosecond laser source as shown in figure 5.2 (b) and (c). Various laser process parameters such as beam scanning speed, ablation time, focus length from target material etc. were same as we used in our previous work (Chapter 4) [Das et al., 2022]. The gas sensor platform with pre-deposited SnO_2 thin film was kept very close to the plasma plume zone (10 mm away from the incident point of the laser beam), as shown in figure 5.2 (b). During ablation the ejected NiO nanoparticles were directly deposited on the top surface of sputtered deposited SnO_2 thin film. Few NiO-deposited samples were prepared by collecting NiO nanoparticles on the top of oxidized silicon wafers to investigate the particle morphology and structural properties.

5.3 Characterization

5.3.1 Structural and morphological characterization of gas sensing materials

The structural characterization of ZnO NPs decorated SnO_2 sample (ZnO/SnO_2) was carried out by X-ray diffraction (XRD) method using CuKα radiation source (Rigaku SmartLab, Rigaku Corporation, Tokyo, Japan) to know about the crystalline phase of the sample. The surface morphology of ZnO NPs decorated SnO_2 sample (ZnO/ SnO_2) and NiO nanoparticles decorated SnO_2 thin film (NiO/SnO_2) were investigated by Field Emission Scanning Electron Microscopy (FESEM, FEI Apreo). The elemental analysis was carried out on ZnO NPs decorated SnO_2 sample (ZnO/ SnO_2) and NiO nanoparticles decorated SnO_2 thin film (NiO/SnO_2) sample using energy dispersive X-ray spectroscopy (EDS) (Model No: FEI Apreo) to know the detailed composition of the sample.

5.3.2 Gas sensing performance test of the fabricated sensors

As we know that metal oxide sensors need heat to work and for that purpose a nichrome heater coil was inserted through the hollow ceramic tube which was used as a source of temperature for the gas sensing layer. The heater works on the principle of Joule heating principle. To produce the heat, heater need to supply current across the two terminals of the heater. To fulfil this need, a source measure unit (Agilent E3632A) was connected with a nichrome (Ni-Cr) heater coil. The heat distribution profile and temperature were measured using an Infrared based thermal imaging camera (AT-Automation Technology GmbH) and the details characterization procedure was discussed in the previous chapter 3. To investigate the formaldehyde gas sensing behaviour, the fabricated ZnO/SnO_2 and (NiO/SnO_2) sensors were kept in an air-tight glass chamber (volume 2.3 L) and the glass chamber was kept on a hotplate to maintain its temperature at 70°C to vaporize the liquid analyte when the liquid analyte was injected into the glass chamber during gas sensing performance test. Before the gas sensing performance test in the presence of various gases, the sensors were preheated continuously for long period (> 2 days) to stabilize the grains of the sensing layer. To measure the change in electrical resistance of the sensor, a LabVIEW based computer program interfaced with a Keithley 2001 multimeter was used. To test the behaviour of the sensor in the presence of various volatile organic compounds (VOCs), the liquid analyte was used as a source. The liquid analyte was injected into the glass chamber via the hole of the top glass-lid using a micropipette. When the liquid analyte came into contact of the hot wall (70°C) of the glass chamber, the analyte gradually converted into vapor and the concentration of VOCs was measured by the standard formula used by Xianfeng Wang et. al. as discussed in detail in chapter 3. Throughout the gas sensing performance test, atmospheric air was used as a purging and reference gas in the test chamber. The gas response value ($\beta = R_a / R_g$) was referred to as the ratio of sensor resistance in ambient air (R_a) to the sensor resistance in the target gas (R_g) towards to a fixed gas concentration. The response (τ_{res}) and recovery time (τ_{rec}) of sensor were calculated by measuring the time taken by the sensor to achieve its baseline resistance change from 90% to 10% in the presence of test gas and 10% to 90% during purging in the ambient air, respectively.

5.4 Results and Discussion

5.4.1 Structural and morphological analysis of gas sensing materials

The top surface morphology of SnO_2 and laser ablated ZnO NPs sensing layer were observed via Field Emission Scanning Electron Microscope (FESEM). In the previous Chapter 4, the FESEM image of laser ablated ZnO nanoparticles was shown [Surajit Das, Jitendra Singh, 2021] and it was already seen that the diameter of the spherical shape ZnO nanoparticles was 31 - 56 nm. Figure 5.3 (a) shows the FESEM image of pristine SnO_2 thin film and 5.3 (b) exhibits the image of ZnO nanoparticles decorated SnO_2 thin film obtained after the drop casting method. It can be seen in FESEM image of figure 5.3 (b) that drop casted laser ablated ZnO NPs are randomly oriented on the sputtered deposited SnO_2 thin film. The EDS spectra of the ZnO nanoparticles decorated SnO_2 sample is shown figure 5.3 (c) and clear peak of Zn is observed in the figure 5.3 (c) of ZnO decorated SnO_2 sample.

The crystal structure of sputtered deposited SnO_2 thin film and ZnO nanoparticles decorated SnO_2 thin film was investigated by X-ray Diffraction (XRD) technique. The test results of XRD are shown in the Figure 5.3 (d). In the bottom of the Figure 5.3 (d), the sharp peaks (110), (101), and (211) of SnO_2 were observed at 2θ = 26.65, 33.9, and 51.9, respectively. The obtained diffraction peaks of the SnO_2 samples are compared with the JCPDS card. No. 41-1445, which are matched with rutile structure of SnO_2 crystals [Cui et al., 2016; Jin et al., 2021]. In the upper portion of the Figure 5.3 (d), an additional diffraction peak was observed at 2θ = 34.6 corresponding to (002) plane of ZnO on the ZnO NPs decorated SnO_2 sample. The obtained diffraction peaks of the test samples are matched with JCPDS card No. 36-1451, which are consistent with the ZnO wurtzite structure [Tian et al., 2015].

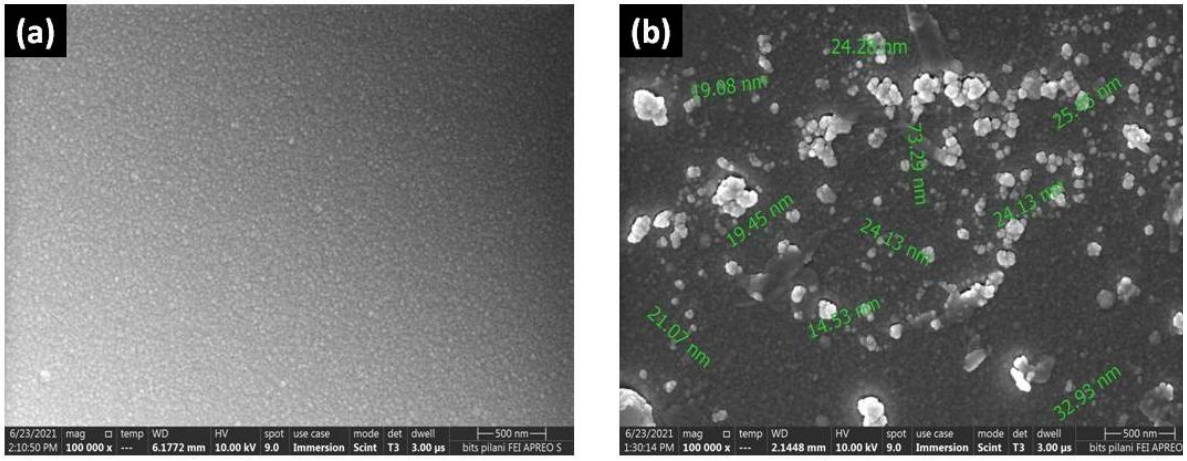

(c)

Element	Weight%	Atomic%
O	21.82	65.1
Sn	67.64	27.20
Zn	10.54	7.70

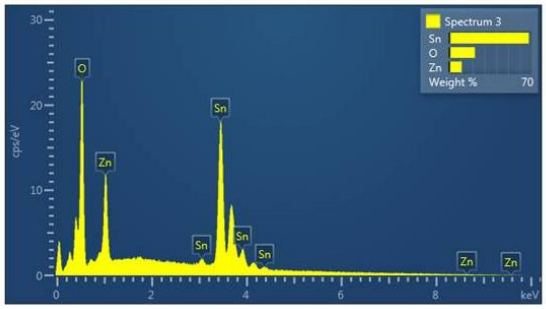

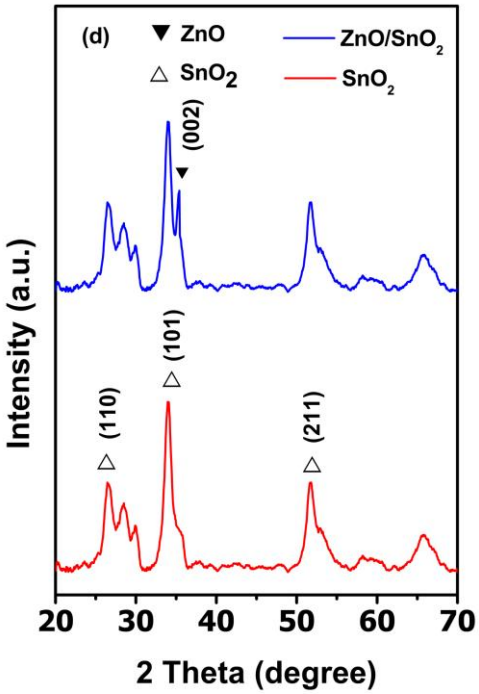

Figure 5.3: (a) FESEM image of pristine SnO_2 thin film. (b) FESEM image of ZnO NPs decorated SnO_2 sample and (c) the corresponding EDS spectra of the ZnO NPs decorated SnO_2 sample shown in (b). (d) XRD patterns of pristine SnO_2 and ZnO decorated SnO_2 sample.

The surface morphology of sputtered deposited pristine SnO_2 thin film and NiO nanoparticles decorated SnO_2 thin film samples was examined via Field Emission Scanning Electron Microscopy (FESEM) as shown in figure 5.4 (a) and (b), respectively. During laser ablation, oxygen (O_2) molecules were dissociated to oxygen atoms due to high-temperature Heat Affected Zone (HAZ) and produced Ni vapor which reacted with surrounding atmospheric oxygen atom. NiO nanoparticles were formed due to the reaction of Ni metal vapor with oxygen (O_2). The gas sensor platform with pre-deposited SnO_2 thin film was placed nearest to the plasma plume area and in the presence of cool ambience, the vapor of NiO nanoparticles came in contact with the alumina tube surface, nucleation and nanoparticles agglomeration occured on top of SnO_2 thin film. At room temperature, loose agglomerate spherical nanoparticles with open structures are formed as shown in figure 5.4 (b). As seen in figure 5.4 (c) that the spherical shape NiO NPs diameters ranged from 45 to 52 nm. The EDS spectra of NiO decorated samples are shown in the figure 5.4 (d) and it reveals that presence of Ni, on the SnO_2 thin film samples.

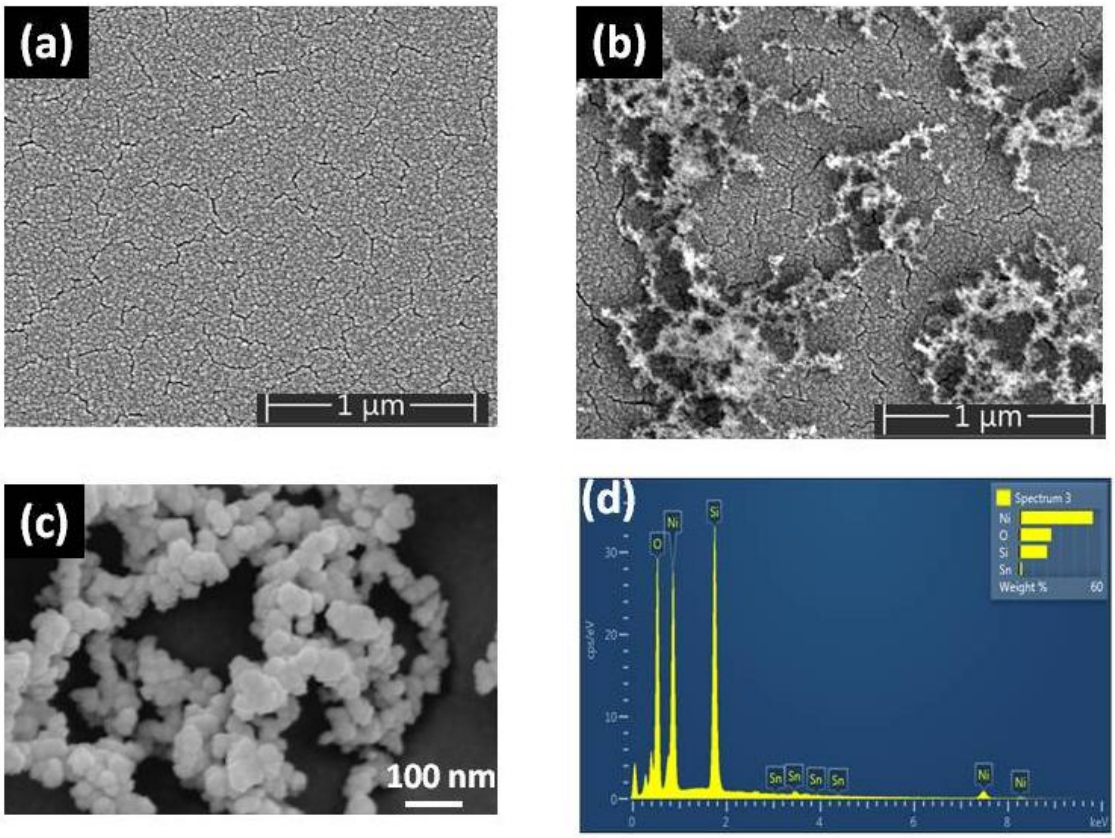

Figure 5.4: (a) FESEM image of pristine SnO_2 thin film. (b) FESEM image of SnO_2 thin film decorated with laser ablated NiO nanoparticles. (c) High-magnification surface image of NiO nanoparticles. (d) EDS analysis of NiO nanoparticles decorated SnO_2 thin film.

5.4.2 Gas response of the fabricated sensors

5.4.2.1 Optimization of the operating temperature of the ZnO/SnO_2 and NiO/SnO_2 sensors

The operating temperature plays an important role in metal oxide based gas sensors. It is well known that the gas response of any chemoresistive metal oxide based gas sensors depends on the working temperature because at higher temperatures (>100°C) the free electrons are generated from the conduction band of the metal oxide [Li et al., 2011b]. As the working temperature increases, the concentration of electrons on the metal oxide surface also increases. So, to start the gas sensing performance test, we have to find out the operating temperature of ZnO/SnO_2 sensor. In our previous studies (Chapter 3), the temperature of the alumina tube heater platform versus applied heating voltage has already been studied. Initially, the sensor resistance (R_a) of ZnO/SnO_2 was measured in atmospheric air at a different working temperature from 100 to 350°C. The test results, sensor resistance versus working temperature, are shown in figure 5.5 (a). It is observed in figure 5.5 (a) that the sensor resistance decreases as the sensing layer temperature rises. It has occurred due to the accumulation of free electrons on the surface of the sensing layer. It is also observed in figure 5.5 (a) that at 100°C the resistance (R_a) of the pure SnO_2 sensor was ~ 1.7 MΩ and ZnO/SnO_2 sensor was ~ 3 MΩ. The baseline resistance (R_a) of ZnO/SnO_2 sensor was comparatively higher (~ 3 MΩ) than SnO_2 sensor at the same temperature (100°C) due to the potential barrier and an EDL formation after decoration of SnO_2 sensor with ZnO nanoparticles. Next, to find the optimum operating temperature of the pristine SnO_2 and ZnO/SnO_2 sensor, the sensor was exposed to a fixed concentration (50 ppm) of formaldehyde gas and the temperature was varied from 100°C to 350°C. The response ($\beta = R_a/R_g$) of the sensor was measured for temperature value from 100°C to 350°C and the temperature difference between two successive measurements was 25°C.

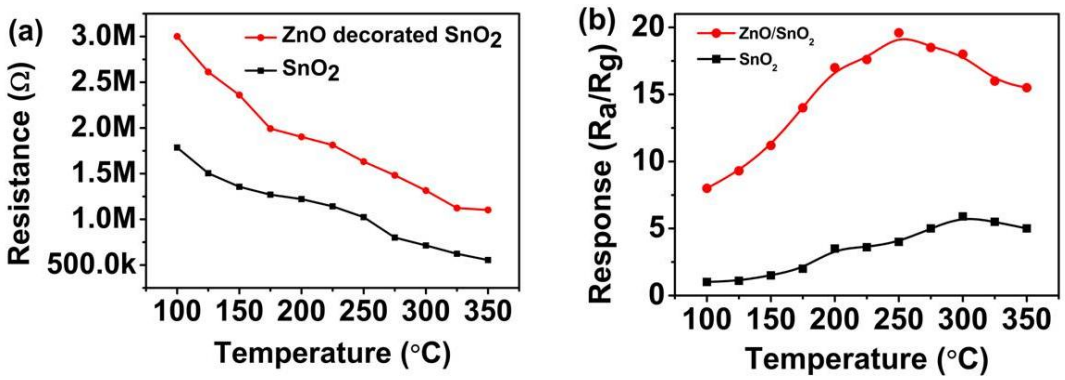

Figure 5.5 : (a) Change of sensor resistance in the air with a temperature of pure SnO_2 (black) and ZnO/SnO_2 (red). (b) Response of pristine SnO_2 (black) and ZnO/SnO_2 (red) to 50 ppm HCHO vapor at different operating temperatures.

Figure 5.5 (b) depicts the sensing response ($\beta = R_a/R_g$) of the SnO_2 and ZnO/SnO_2 towards 50 ppm formaldehyde gas at various working temperatures from 100°C to 350°C. It can be seen in figure 5.5 (b) that first, the response of the SnO_2 and ZnO/SnO_2 sensor gradually increases as the temperature increases and then decreases as the working temperature rises. As the temperature increases, the absorption rate of molecular oxygen (O_2^- , O^- and O^{2-} species) on the surface of the sensing layer increases [Li et al., 2019a] but after reaching the saturation point (operating temperature), the desorption process starts due to the lack of oxygen vacancies on the surface of the sensing layer. In figure 5.5 (b), we have observed that towards 50 ppm of formaldehyde, pristine SnO_2 sensor shows an optimum response of about 5.7 at 300°C and the ZnO/SnO_2 sensor shows an optimum response of about 19.6 at 250°C. It is also noticed from figure 5.5 (b) that the response of the ZnO/SnO_2 sensor enhances (β =19.6) at a lower working temperature (250°C) compared to a pristine SnO_2 sensor. This enhancement of response was caused by ZnO/SnO_2 sensor mainly due to the heterojunction effect and Fermi Level modulation where the charge transfer occurred at the SnO_2 and ZnO material interface. In this chapter, we have tested the gas sensing performance of ZnO/SnO_2 and SnO_2 sensors at 250°C, 300°C, respectively.

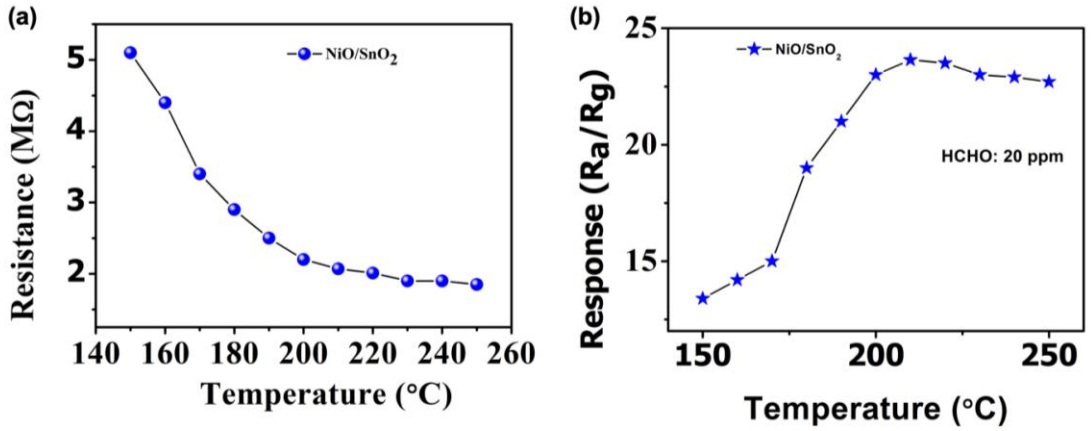

Figure 5.6 : (a) Change in sensor resistance of NiO/SnO_2 sensor as a function of operating temperature. (b) Gas response versus operating temperature of NiO/SnO_2 sensor to 20 ppm HCHO vapor.

The change in sensor resistance versus the working temperature of *p*-NiO/*n*-SnO_2 is shown in figure 5.6 (a). The working temperature was changed from 150 to 250°C. It is observed in figure 5.6 (a) that the baseline resistance of the *p*-NiO/*n*-SnO_2 sensor was ~ 5.1 MΩ at 150°C

in ambient air and the baseline resistance decreases as the working temperature increases. At 250°C working temperature, the baseline resistance was 1.85 MΩ. Before starting of the gas sensing performance test, we have to measure the operating temperature of the sensor. For that purpose, we also measured the response of the *p*-NiO/*n*-SnO_2 sensor to a fixed concentration (20 ppm) of formaldehyde gas by varying the temperature from 150 to 250°C. The response (R_a/R_g) vs. operating temperature results of the *p*-NiO/*n*-SnO_2 sensor is shown in the figure 5.6 (b). We have already studied the operating temperature of the pristine SnO_2 sensor in our previous chapter 4 and we found the optimal response of 4.62 at a much higher temperature of 300°C [S. Das et al., 2021]. But, after the decoration of NiO nanoparticles on the SnO_2 sensor, the *p*-NiO/*n*-SnO_2 sensors showed its optimum response of about 23.64 at 210°C. However, the response of the *p*-NiO/*n*-SnO_2 sensors then decreased, although the temperature increased. This phenomenon was already discussed in the previous chapter 4. From figure 5.6 (b), it is seen that the NiO/SnO_2 sensor shows maximum response at 210°C.

5.4.2.2 Static response behaviour of the ZnO/SnO_2 and NiO/SnO_2 sensors

The static response ($\beta = R_a/R_g$) of ZnO/SnO_2 sensor was studied in a closed glass chamber by placing the fabricated sensors in the chamber with varying concentrations of formaldehyde. The sensor resistance and response ($\beta = R_a/R_g$) of ZnO/SnO_2 sensor are presented in figure 5.7 (a) and (b), respectively. From figure 5.7 (a), it has been observed that the resistance of the ZnO/SnO_2 sensor decreases rapidly in the presence of formaldehyde gas from 0.25 to 200 ppm. Moreover, it is also observed that the baseline resistance of the ZnO/SnO_2 sensor recovered to its initial state rapidly when the formaldehyde vapor runs away from the sensor surface. Furthermore, it was also observed in figure 5.7 (b) that the ZnO/SnO_2 sensor showed a good response (β) towards the various concentrations of formaldehyde gases from 0.25 to 200 ppm and at 200 ppm of formaldehyde gas, the sensor shows its maximum response (β) of about 50.

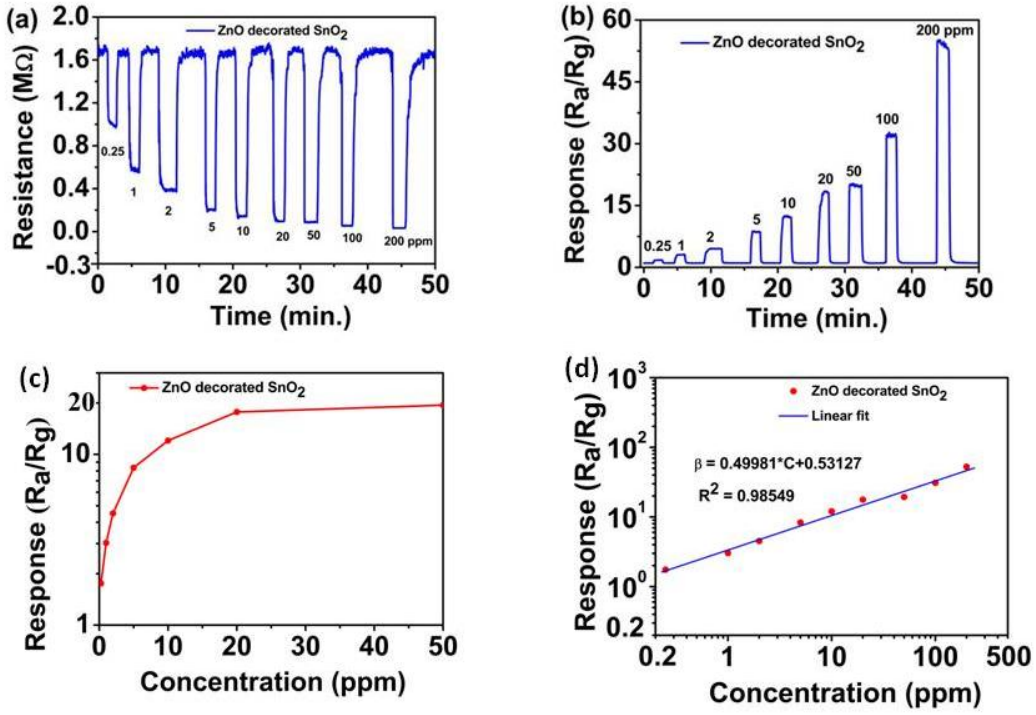

Figure 5.7: (a) Change of resistance of ZnO/SnO_2 sensor towards 0.25 to 200 ppm HCHO. (b) Static gas response of ZnO/SnO_2 sensor at various gas concentrations from 0.25 to 200 ppm. (c) Response versus concentration of ZnO/SnO_2 sensor towards different concentrations of HCHO range 0.5 to 50 ppm. (d) ZnO/SnO_2 sensor response fitting curves at optimal working temperature 250°C.

Calculation of the limit of detection (LoD) is also a very important task during the gas sensing performance test of the fabricated sensors. These parameters are calculated from the previous experimental results during the study of the static response behaviour of the

ZnO/SnO_2 sensors at various concentrations levels from 0.25 – 200 ppm, as shown in figure 5.7 (b). To find the Limit of Detection (LoD) of the ZnO/SnO_2 sensor, the response graphs of figure 5.7 (b), were used. It can be seen in figure 5.7 (b) that in the presence of 0.25 ppm formaldehyde gas the ZnO/SnO_2 sensor exhibit response (β) of 1.74. For potential application of gas sensor in real life, the response (β) value towards formaldehyde should be equal or more than 1.2. So, from the Figure 5.7 (b) the theoretical limit of detection (LoD) of the ZnO/SnO_2 sensor can be extracted as $\leq$ 0.25 ppm towards formaldehyde [Castro-Hurtado et al., 2011].

The response versus formaldehyde concentration of ZnO/SnO_2 sensors is shown in figure 5.7 (c). It can be seen in figure 5.7 (c) that the response of ZnO/SnO_2 sensor increases with increasing of formaldehyde (HCHO) concentration continuously up to 50 ppm. Figure 5.7 (c) shows that the rate of increase in response of ZnO/SnO_2 sensor was increased rapidly below 20 ppm, slower during 20 and 30 ppm and then saturated after 30 ppm with further increasing the formaldehyde (HCHO) concentration.

From these values, we plotted the linear fit model of the ZnO/SnO_2 sensor in figure 5.7 (d). The figure 5.7 (d) present the gas the response ($\beta = R_a/R_g$) versus various concentration of formaldehyde level . The linear fitting curve follows the following equation (5.1):

$$\beta = mC + k \qquad (5.1)$$

Where, β represents the gas response of the sensor, m presents the gas response coefficient, C stands for the gas concentration of HCHO and k is a constant value. From the figure 5.7 (d), it is observed that the test results data and the fitting relationship show good agreement. From the figure 5.7 (d), we obtained the response value (β) of ZnO/SnO_2 sensor from the fitting curve model as follows: β = 0.49981*C + 0.53127 with the correlative coefficient (R^2) of 0.98549. From figure 5.7 (d), based on the linear fit model, the sensitivity of ZnO/SnO_2 sensor was 0.49981 ppm^{-1}. We can observe from these results that the sensitivity of ZnO/SnO_2 heterojunction sensor is much higher (0.53127 ppm^{-1}) than the pristine SnO_2 sensor (0.19 ppm^{-1}) alone, as discussed in the previous chapter 4. Hence, the high linear relationship model of ZnO/SnO_2 sensor between the change in sensor response with different concentrations of formaldehyde gas shows the great impact on the development of real-time formaldehyde gas measurement systems in our daily life.

Figure 5.8 (a) shows the static response-recovery cycles of NiO/SnO_2 sensors to different concentrations of HCHO from 0.5 to 50 ppm at its operating temperature 210°C. As seen in figure 5.8 (a), after injection of formaldehyde (HCHO) vapor into the test chamber, the resistance of the sensor decreases exponentially from its baseline value (~ 2.21 MΩ) and within seconds sensor reaches its steady state, whereas sensor resistance reaches to its original baseline level after opening the test chamber to air. It is also seen in figure 5.8 (a) that the sensor resistance value has been changed to 0.29 MΩ, 0.229 MΩ, 0.153 MΩ, 0.1 MΩ, 0.096 MΩ, 0.088MΩ, 0.080 MΩ, 0.075 MΩ when the sensor was exposed with 0.5, 1, 5, 10, 20, 30, 40 and 50 ppm of HCHO, respectively. Figure 5.8 (b) shows the response (R_a/R_g) of the NiO/SnO_2 sensors. The sensor exhibits response value of 7.4, 10.18, 20.33, 22.87, 24.54, 26.53, 29.14 and 31.04 to 0.5, 1, 5, 10, 20, 30, 40 and 50 ppm formaldehyde (HCHO), respectively.

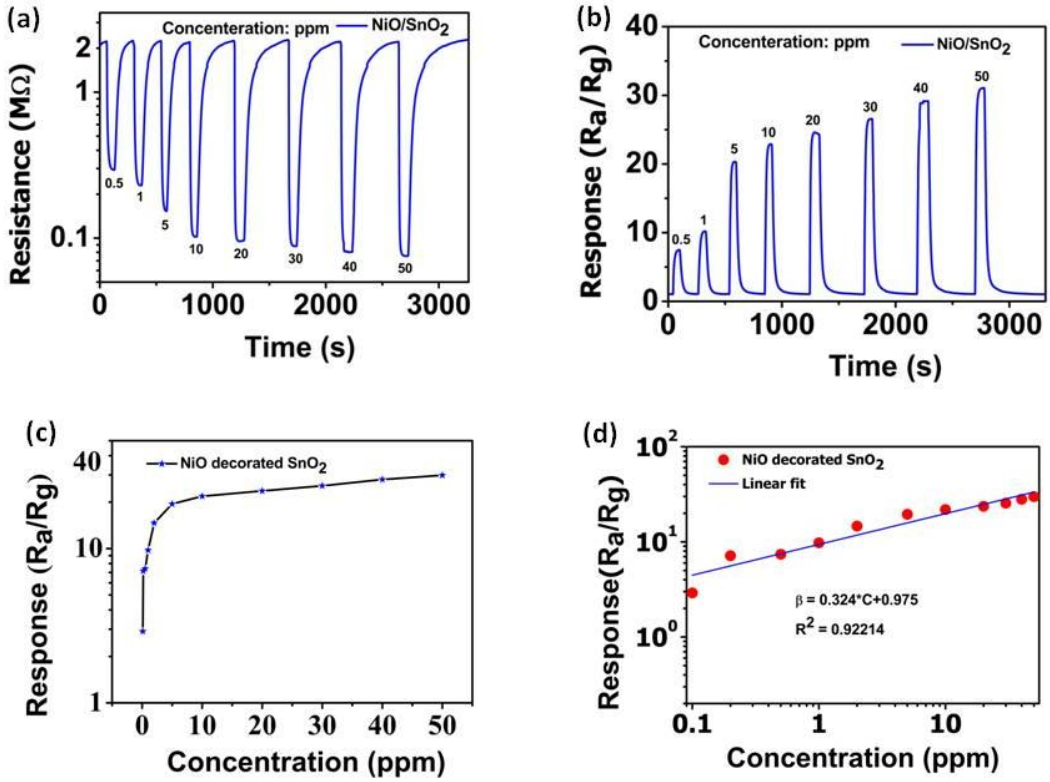

Figure 5.8: (a) Change in resistance of NiO/SnO_2 sensor towards different concentrations of HCHO range 0.5 ppm to 50 ppm. (b) Response of NiO/SnO_2 sensor towards different concentration of HCHO range 0.5 to 50 ppm. (c) Response versus concentration of NiO/SnO_2 sensor towards different concentrations of HCHO range 0.5 to 50 ppm. (d) NiO/ SnO_2 sensor response fitting curves at optimal working temperature 210°C.

Calculation of the limit of detection (LoD) is also a very important task during the gas sensing performance test of the fabricated sensors. These parameters are calculated from the previous experimental results during the study of the static response behaviour of the ZnO/SnO_2 sensors at various concentration levels from 0.5 –50 ppm as shown in figure 5.8 (b). From the figure 5.8 (b), we have seen that the sensor shows it response of 7.64 at 0.5 ppm HCHO and the sensor shows it response of 2.91 at 0.1 ppm of HCHO. So, the limit of detection (LoD) of NiO/SnO_2 is < 0.1 which is lower than our previously made SnO_2 and ZnO/SnO_2 sensor. From this comparison, the present NiO/SnO_2 sensors exhibit obvious advantages over pure SnO_2 and ZnO/SnO_2 sensor.

Fig 5.8 (c) indicates the sensor response as a function of the concentration of HCHO vapors for NiO/SnO_2. We have observed from figure 5.8 (c) that the response of SnO_2 sensors increases almost linearly with increasing concentration of HCHO vapor from 0.1-50 ppm but for the NiO/SnO_2 sensor the response increases exponentially.

The log-log plot of sensor response against HCHO concentration for NiO/SnO_2 sensor is shown in Fig 5.8 (d). From these values, we plotted the linear fit model of the NiO/SnO_2 sensor in figure 5.8 (d). The figure 5.8 (d) presents the gas the response ($\beta = R_a/R_g$) versus various concentration of formaldehyde level of the NiO/SnO_2 sensors. The linear fitting curve follows the equation (5.1) as discussed in previous section. From the figure 5.8 (d), it is observed that the test results data and the fitting relationship show good agreement. From figure 5.8 (d), we obtained the response value (β) of NiO/SnO_2 sensor from the fitting curve model as follows: as follows: β = 0.324*C + 0.975 with the correlative coefficient (R^2) of 0.92214 and from the linear fit model (Figure 5.8 (d)), we have found the sensitivity of NiO/SnO_2 sensor is 0.324 ppm^{-1}.

5.4.2.3 Response and recovery time of the ZnO/SnO_2 and NiO/SnO_2 sensors

To find the response (τ_{res}) and recovery time τ_{rec}) of the metal oxide based sensor, the

static response of the ZnO/SnO_2 and NiO/SnO_2 sensors was observed. For this purpose, the change in sensor resistance with time under a fixed concentration of formaldehyde gas was measured. The response and recovery graph of the ZnO/SnO_2 and NiO/SnO_2 sensors are presented in figure 5.9 (a) and (b), respectively. The response (τ_{res}) time is defined as the time taken by the gas sensor to change its baseline resistance (R_a) value from 10% to 90% of the final value in the presence of target gas molecules and recovery time (τ_{rec}) is the time taken by the sensor to recover 90% of its baseline resistance value (R_a) during when the source gas is removed from the chamber. The response (τ_{res}) and recovery time (τ_{rec}) of the ZnO/SnO_2 and NiO/SnO_2 are calculated from figure 5.9 (a) and (b), respectively. It is seen from the figure 5.9 (a) that ZnO/SnO_2 shows the response (τ_{res}) and recovery time (τ_{rec}) of 4 s, 30 s, respectively, in the presence of 50 ppm HCHO. The NiO/SnO_2 sensor was exposed to 20 ppm HCHO and the response (τ_{res}) and recovery time (τ_{rec}) of the NiO/SnO_2 sensor were calculated from figure 5.9 (b) and the response (τ_{res}) and recovery time (τ_{rec}) are 3 s, 91 s, respectively. From these value, it is seen that the decoration of NiO nanoparticles on SnO_2 thin film reduced the response and recovery time to some extent.

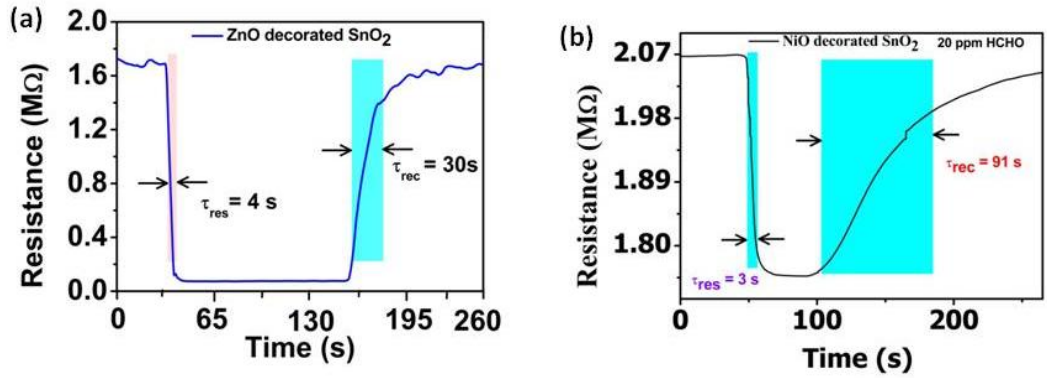

Figure 5.9: (a) Response and recovery graph of ZnO/SnO_2 towards 50 ppm of HCHO. (b) Response and recovery graph of NiO/SnO_2 towards 20 ppm of HCHO.

5.4.2.4 Short-term repeatability of the ZnO/SnO_2 and NiO/SnO_2 sensor

Furthermore, measuring the short-term repeatability of the metal oxide sensors is also a key factor to test the feasibility and real-life applications of fabricated sensors. In the presence of a fixed concentration of formaldehyde gas, the short-term repeatability experiment was carried out and the test cycles were continued ten times. Figure 5.10 (a) and (b) show the short-term repeatability results of the ZnO/SnO_2 and NiO/SnO_2 sensors, respectively. During the test, we maintained the condition as we followed in our previous chapters 4. After recovering the baseline resistance to its original value, the test was repeated ten times by exposing the sensor to the same concentration of formaldehyde. It is observed in figure 5.10 (a) and (b) that for each successive measurement, the variation of ZnO/SnO_2 and NiO/SnO_2 sensor resistance is almost identical to 50 and 20 ppm of HCHO, respectively, which exhibit excellent reproducibility of the fabricated sensors [Gu et al., 2017].

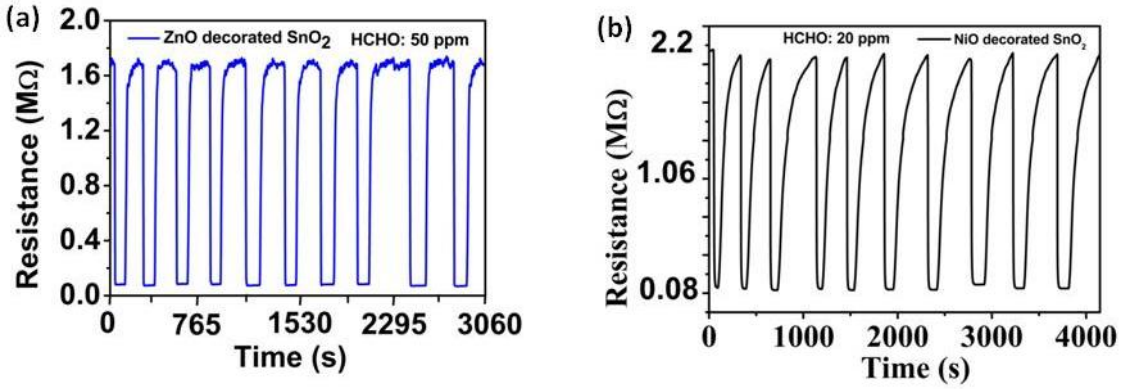

Figure 5.10 : (a) Short-term repeatability test of ZnO/SnO_2 sensor towards 50 ppm of HCHO. (b) Short-term repeatability test of NiO/SnO_2 sensor towards 20 ppm of HCHO.

5.4.2.5 Long-term reliability of NiO/SnO_2 sensors

The long-term reliability of ZnO/SnO_2 and NiO/SnO_2 sensors was investigated by measuring the response of the sensors towards fixed formaldehyde gas over 30-day (RH 70%) period of time. The long-term reliability test results of ZnO/SnO_2 and NiO/SnO_2 sensors are shown in figure 5.11 (a) and (b), respectively. To collect the data, daily, the ZnO/SnO_2 and NiO/SnO_2 sensors were exposed with 50 ppm and 20 ppm of formaldehyde gas, respectively. After gathering the 30 days of data, we plotted the data in figure 5.11 (a) and we have seen that there is a negligible change in response over 30 days. The long-term stability test of the ZnO/SnO_2 sensors confirms that the stability of the ZnO decorated SnO_2 sensor is excellent in the long-term detection of formaldehyde which is essential for real life application. We have also studied the long-term reliability test of the NiO/SnO_2 sensor towards a fixed HCHO concentration of 20 ppm for 30 days. For that purpose, NiO/SnO_2 sensor was exposed to 20 ppm of HCHO daily and measured the response as shown in figure 5.11 (b).

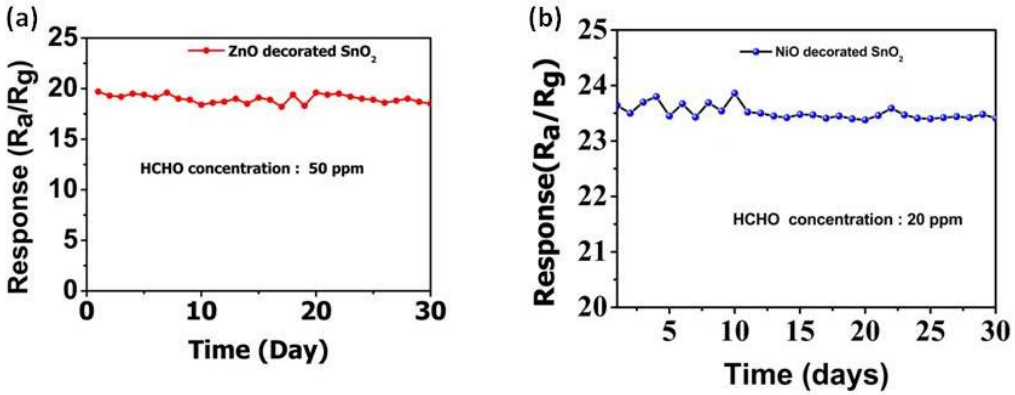

Figure 5.11 : (a) Long-term stability of ZnO/SnO_2 sensors towards 50 ppm HCHO over the period of 30 days. (b) Long-term reliability test of the NiO/SnO_2 sensor towards 20 ppm of HCHO for 30 days.

5.4.2.6 Cross-response of ZnO/SnO_2 and NiO/SnO_2 sensors to other VOCs

To study the selectivity of the metal oxide sensor, the fabricated ZnO/SnO_2 and NiO/SnO_2 sensors were exposed with various volatile organic compounds (VOCs) such as formaldehyde, methanol, ethanol, acetone, TCE and isopropanol etc. and the concentration of each VOCs was maintain 50 ppm. To measure the selectivity of the sensor is very important because this property shows the sensor's ability to detect target gas in real-life applications. After studying the response of the ZnO/SnO_2 and NiO/SnO_2 sensors, the results are plotted in figure 5.12 (a) and (b) and it is observed that the ZnO/SnO_2 sensor exhibits a high response of

about 20 with the 50 ppm concentration of formaldehyde. On the other hand, the response of the ZnO/SnO_2 sensor to other volatile organic compounds (VOCs), such as methanol, ethanol, acetone, TCE and isopropanol, are 8, 7.5, 4, 2.5 and 7, respectively. Moreover, SnO_2 sensor shows a lower response to formaldehyde and other VOCs, as seen in figure 5.12 (a). So, compared with SnO_2 sensor, the ZnO/SnO_2 sensor has an excellent selectivity to HCHO.

The response ($\beta = R_a/R_g$) versus HCHO concentration of NiO/SnO_2 and SnO_2 were shown in figure 5.12 (b) and the response of NiO/SnO_2 sensor is higher compared than SnO_2 sensor. In order to study the selectivity of the gas sensor, the sensor response was tested towards various VOCs at a fixed value of 50 ppm concentration at an operating temperature 210°C. The sensor responses ($\beta = R_a/R_g$) to the methanol (CH_3OH), ethanol (C_2H_5OH), formaldehyde (HCHO), acetone (C_3H_6O), TCE (C_2HCl_3) and Isopropanol (C_3H_8O) were 11.92, 11.1, 29.8, 5.96, 4.47, 10.43, respectively as shown in figure 5.12 (b). It is clearly seen that the sensor shows a much higher response to formaldehyde gas compared to the other VOCs. The previous work reported that the pure SnO_2 sensor shows not much selective response compared that NiO/SnO_2 sensor and values were 3.5, 3.2, 5.9, 2, 1.5, and 3, respectively.

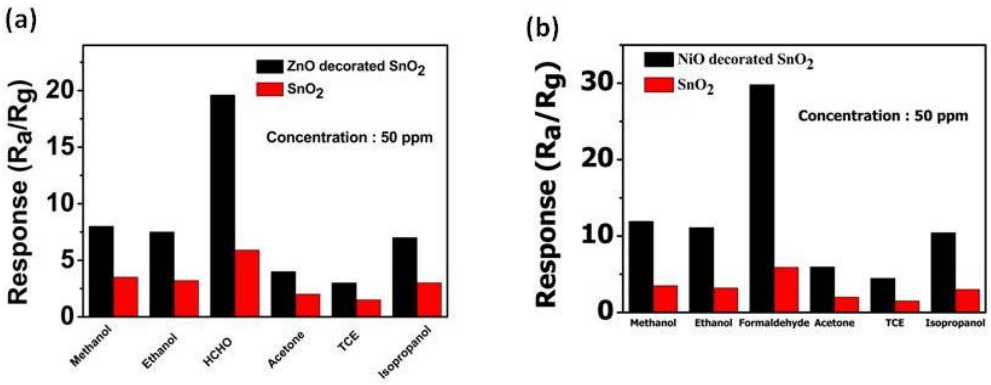

Figure 5.12 : (a) Cross-response of pristine SnO_2 and ZnO/SnO_2 sensors towards 50 ppm concentration of HCHO and other VOCs. (b) Cross-response of SnO_2 and NiO/SnO_2 sensor towards 50 ppm concentration of HCHO and other VOCs.

5.4.2.7 Effect of humidity

During the gas sensing performance test, ambient air with 70% Relative humidly (RH) was used as both reference and diluting gas. To study the effect of formaldehyde gas (HCHO), commercially available formalin solution (37 wt % formaldehyde gas in water) has been used as a source of formaldehyde gas which contains water. So, it is necessary to study the effect of humidity on sensors. During the test, after baseline stabilization, a small amount of water was injected inside the test chamber using micropipette which was vaporized by the hot wall of the glass chamber. And the change of baseline resistance was measured as shown in figure 5.13 (a) and (b). Form the result, we have seen that base line resistance (R_S) of SnO_2 (Figure 5.13 (a)) and ZnO/SnO_2 sensors (Figure 5.13 (b)) have been changed to 12% and 14%. More number of hydroxyl ions were absorbed on the available site on the sensor surface due to an increase in humidity and hence, conductivity was increased. We have also investigated the humidity effect on NiO/SnO_2 sensors but there is a negligible change in baseline resistance at 95% RH.

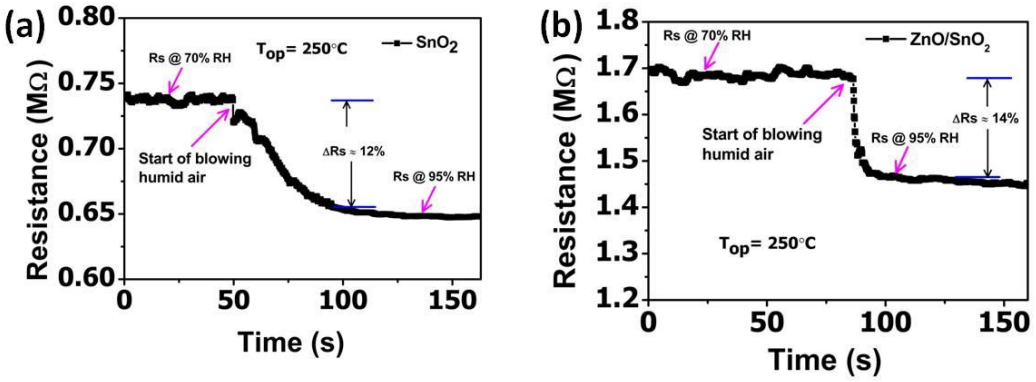

Figure 5.13 : (a) Change in baseline resistance due to increase of relative humidity in SnO_2 sensor. (b) Change in baseline resistance due to increase of relative humidity in ZnO/SnO_2 sensor.

Table 5.1 and 5.2 show the formaldehyde gas sensing performance comparison between the previously reported metal oxide based sensors having p-n or n-n heterojunctions and the sensor developed (ZnO/SnO_2 and NiO/SnO_2) in this chapter 5.

Table 5.1: Comparison of various heterojunction based metal oxide sensors to HCHO gas with our fabricated ZnO/SnO_2 sensor.

Sensing materials	Synthesis Process	Response /concentration (ppm)	Response/ recovery time (s)	Operating temperature (°C)	Ref.
CuO /SnO_2	solution processing and atomic layer deposition	2.42 / 50	52/80 to 6 ppm HCHO	250	[Ju et al., 2015]
AgO/ SnO_2	FSP and Spin coating	495/ 2000	1.7 to 2000 ppm HCHO	350	[Ju et al., 2014]
NiO/SnO_2	electrospinning process.	20/ 100	50/80 to 10 ppm HCHO	200	[Xu et al., 2016]
NiO/ SnO_2	hydrothermal route	40 / 100	28/115 to 100 ppm HCHO	100	[Guo et al., 2014]
NiO/ SnO_2	chemical solution route	27.6	5/15	240	[Wang et al., 2012]
SnO/SnO_2	Hydrothermal	80.9/ 50	7/27	120	[Dey, 2018]
Zn_2SnO_4/SnO_2	hydrothermal synthesis	8.1 /100	35/78 to 1000 ppm HCHO	162	[Simon et al., 2001]
In_2O_3/SnO_2	electrospinning process	18.9 / 50	-	375	[Chung et al., 2013]
SnO_2 /ZnO	Sputtering /Atomic layer deposition (ALD)	38.2/ 20	12/24 to 1000 ppm HCHO	200	[Du et al., 2012]
Au - ZnO/SnO_2	Hydrothermal /Atomic layer deposition (ALD) and sputtering	12.4/50	1.2/75 to 50 ppm TEA	40	[Meng et al., 2018c]
ZnO/SnO_2	Laser ablation/ Sputtering	20/50	4/30 to 50 ppm HCHO	250	This work

Table 5.2 : Comparison of various gas sensing properties of heterojunction based sensors with our fabricated NiO/SnO_2 based sensor.

Sensing materials	Synthesis Process	Response / Concentration	Response / recovery time (s)	Operating temperature (°C)	Ref.
NiO/ SnO_2	FSP and Spin coating	26.03/ 50 Ppm HCHO	1.7 to 2000 ppm HCHO	100	[Zhang et al., 2016]
NiO/ SnO_2	hydrothermal	39.2 / 100 ppm HCHO	28/115 to 100 ppm HCHO	100	[Meng et al., 2018b]
NiO/SnO_2	Hydrothermal/PLD	48.6 /10 ppm TEA	50/80 to 10 ppm triethylamine	200	[Ju et al., 2015]
NiO/ SnO_2	chemical solution route	7.9 / 100 ppm Ethanol	5/15	250	[Fang et l., 2017]
NiO / SnO_2	hydrothermal route	27.6 / 100 ppm HCHO	5/15 50 ppm HCHO	240	[Gu et al., 2017]
NiO/SnO_2	Hydrothermal	80.9/ 50 ppm HCHO	7/27	120	[Din et al., 2020]
NiO/SnO_2	hydrothermal synthesis	6 /5 ppm HCHO	35/78 to 1000 ppm HCHO	162	[Pascariu et al., 2016]
NiO/ SnO_2	Electrospinning method	20 / 100 ppm HCHO	50/80 to 10 ppm	200	[Zheng et al., 2011]
NiO/SnO_2	electrospinning process	18.9 / 50 to Acetone	2/9 to 50 ppm acetone	300	[Hu et al., 2018]
NiO/SnO_2	electrospinning process	38.2/ 20 Acetone	12/24 to 1000 Acetone	200	[Tang et al., 2016]
NiO/10% Sn	Chemical solution	145/100 ppm HCHO	-	225	[Wang et al., 2017]
$NGQD/TiO_2$	Hydrothermal synthesis	9.1 /100 ppb HCHO	18 / 20 (100 ppb HCHO)	150	[Shao et al., 2020]
NiO/SnO_2	Laser ablation/Sputtering	29.8/50 HCHO	18 s/105 to 20 ppm HCHO	210	This work

5.5 Conclusion

In summary, a highly sensitive ZnO/SnO_2 heterojunction based formaldehyde sensor has been fabricated via decoration of sputtered deposited SnO_2 thin film with laser-ablated ZnO nanoparticles. For the decoration with ZnO nanoparticles over the SnO_2 thin film, a ZnO nanoparticles enriched colloidal solution was formed. In this work, we have developed a reliable one-step synthesis and decoration method. The ultrasensitive ZnO/SnO_2 n-n heterojunction based sensor can be made directly on a commercially available gas sensor platform which is scalable with rapid prototype-building capability in a very short time and the synthesis process of ZnO nanoparticles is free from hazardous chemicals. After the decoration of ZnO NPs on SnO_2 sensor, it exhibited high sensitivity (~ 20), quick response (4 s) and recovery time (30 s) with good reliability towards 50 ppm formaldehyde with a sub-ppm detection limit (0.25 ppm) at lower operating temperature (250°C) compared to that of pure SnO_2 sensor. Additionally, this novel chemical-free nanoparticle synthesis method demonstrates the feasibility of making a simple and economical sensor fabrication method which can replace the traditional fabrication process in the future. Moreover, in this chapter, we have synthesized p-type NiO functional nanoparticles using the laser ablation method to form NiO/SnO_2 heterojunction-based sensor via decoration of laser ablated NiO nanoparticles on sputtered deposited SnO_2 thin film. It was observed that NiO functional materials improved the selectivity and sensitivity towards formaldehyde. It was observed that the fabricated sensor exhibited enhanced response (R_a/R_g) of 31.04 towards 50 ppm HCHO with fast response (3 s) and recovery (91 s) time at lower operating temperature (210°C) with good selectivity, higher sensitivity, and lower detection limit compared to pure SnO_2 and ZnO/SnO_2 sensor. This work also shows a new decoration method which is based on laser ablation technique and it has great potential to use as an alternative chemical-free route to fabricate high performance pristine or heterojunction-based metal oxide sensors for the detection of formaldehyde or other toxic and hazardous gases. Here, we used an in-house designed customized laser system for the ablation of metal pellet to make it cost-effective and affordable. The synthesis time is very low so rapid prototype building is possible with less time.

Understanding the formaldehyde gas sensing mechanism and calculation of various gas sensing parameters such as response time (τ_{res}), recovery time (τ_{rec}), surface coverage (θ) and, adsorption (K_a) and desorption rate constant (K_d) are very important. Hence, in the next chapter, we will discuss the gas sensing mechanism and modeling part through which various gas sensing parametrers can be extracted from experimental data using the Langmuir gas adsorption-desorption model via curve fitting method.

…